Applied Surface Science 255 (2009) 9006–9009

Contents lists available at ScienceDirect

Applied Surface Science

journal homepage: www.elsevier.com/locate/apsusc

$ZnO:CeO_2$-based nanopowders with low catalytic activity as UV absorbers

Juliana Fonseca de Lima, Renata Figueredo Martins, Cláudio Roberto Neri, Osvaldo Antonio Serra *

Department of Chemistry, FFCLRP, USP, Av. Bandeirantes 3900, CEP 14040-901 Ribeirão Preto, SP, Brazil

ARTICLE INFO

Article history:
Received 24 April 2009
Received in revised form 17 June 2009
Accepted 18 June 2009
Available online 24 June 2009

Keywords:
Cerium oxide
Ceria
Zinc oxide
Rare earth
Sunscreen
UV protection

ABSTRACT

Ultrafine systems of zinc oxide and cerium oxide for use as ultraviolet filter were synthesized by a non-alkoxide sol–gel process at different temperatures, to obtain solid materials (40 and 70 °C), that were characterized by X-ray diffraction, scanning electron microscopy, UV–vis reflectance. Their catalytic and photocatalytic activities were also evaluated. $ZnO:CeO_2$ systems present higher UV absorption and transparency in the visible region. The photocatalytic activity of $ZnO:CeO_2$ systems for the oxidation of organic materials is much smaller than that of titania, ceria and zinc oxide, suggesting that $ZnO:CeO_2$ systems are promising candidates for use as optical materials in UV-filters.

© 2009 Elsevier B.V. All rights reserved.

1. Introduction

Materials based on cerium oxide have been extensively used as glass polishing materials [1], oxygen ion conductor in solid oxide fuel cells (SOFCs) [2], gas sensors [3], UV absorbent [4], and catalytic supports or promoter for automotive exhaust gas conversion reaction [5]. The fine powder of cerium oxide has suitable features for use in personal care products based on inorganic materials for blocking of ultraviolet radiation.

The optical properties of ceria-based materials were investigated in order to characterize their potential abilities as inorganic UV absorbents. Fine particles of titanium oxide and zinc oxide are effective solar protectors, being the main compounds used as inorganic anti-UV, currently used in the cosmetic industry [6,7]. Their high refractive index, however, may give the skin a peculiar look. In addition, their high photocatalytic activity facilitates generation of reactive oxygen species, which can oxidize and degrade other ingredients in the formulation. In contrast, cerium oxide has a low refractive index and is relatively transparent to visible light, not to mention its excellent properties concerning absorption of UV radiation and its lower photocatalytic activity compared with TiO_2 and ZnO. Nevertheless, because of its catalytic activity for the oxidation of organic materials, CeO_2 has been rarely used for commercial purposes such as sunscreen. The use of cerium oxide together with zinc oxide should reduce the catalytic and photocatalytic activities, i.e., the evolution of oxygen molecules, thus preventing degradation of organic materials [8].

Fine $ZnO:CeO_2$-based particles with very small size exhibit unique UV absorbing ability, high stability at high temperatures, high hardness, and low activity as catalyst [9].

Numerous techniques have been proposed for the synthesis of nanosized CeO_2 particles with promising control of properties [10]. The large-scale production of powders needs to be economically feasible and should not be complex. Sol–gel method is easily reproducible and applicable to the fabrication of products in large industrial scale and at a low cost [9].

In the present work, the ultrafine systems of zinc oxide and cerium oxide were prepared by a non-alkoxide sol–gel method, by the use of cerium nitrate and zinc acetate precursors and lactic acid as stabilizer.

2. Experimental

Solid system $ZnO:CeO_2$ was synthesized from an ethanolic suspension of $Zn(CH_3COO)_2{\cdot}2H_2O$ (0.4 mol L^{-1}) and cerium nitrate, heated under reflux with successive additions of lactic acid until total dissolution of $Zn(CH_3COO)_2{\cdot}2H_2O$ and formation of a stable and transparent sol. The Zn/Ce molar ratio in solution was 9:1. The pure oxides (ZnO, TiO_2, CeO_2) were purchased from Aldrich.

The procedure was performed twice, so that two samples (sols) could be submitted to drying at different temperatures, namely 40 and 70 °C, and the two products could be compared. The powders were calcined at 600 °C for 2 h until complete elimination of the organic material.

* Corresponding author. Tel.: +55 16 3602 3746.
E-mail address: osaserra@usp.br (O.A. Serra).

0169-4332/$ – see front matter © 2009 Elsevier B.V. All rights reserved.
doi:10.1016/j.apsusc.2009.06.071

The crystalline phase was analyzed by X-ray diffraction, XRD, on a SIEMENS D5000 X-ray diffraction analyzer. The size distribution and powder shapes were observed by scanning electron microscopy, SEM on a scanning electron microscope Zeiss EVO 50. For diffuse reflectance spectroscopic (DRS) measurements, the powders were ground in agate mortar and compacted in a black holder. A spectrofluorometer SPEX-FLUOROLOG 3 was used to record DRS spectra by synchronously scanning the excitation and emission monochromators [11].

The catalytic and photocatalytic activities for oxidation of organic materials were determined by the conductometric determination method (Rancimat® method) [6] using castor oil as the oxidizing material. For determination of the photocatalytic activity, the samples were submitted to irradiation using a xenon lamp (Xenarc D–H4R–35W). The powder samples (30 mg) were then mixed with 3.0 mL of castor oil and maintained at 120 °C under of air flow, and the air was introduced into the deionized water attached to the electric conductivity measurement cell. For evaluation of the catalytic and photocatalytic activities of the samples, the increase in the electric conductivity of the deionized water was measured by trapping volatile molecules coming from the oxidation of heated castor oil.

3. Results and discussion

The diffractograms of the samples synthesized by the non-alkoxide sol–gel method at drying temperatures of 40 and 70 °C display reflection peaks characteristic of crystalline samples. For both powders, the reflection planes perfectly match the indexed CeO_2: cubic system, unit cell, and cubic face centered space group *Fm*3*m* (225); and ZnO: hexagonal system, primitive unit cell, and space group *P*63*mc* (186) [12]. No peak due to any other phase was observed. The X-ray patterns of CeO_2, ZnO, and CeO_2:ZnO are depicted in Fig. 1.

Fig. 1 shows that the synthesized sample ZnO:CeO_2 (40 °C) has less intense peaks compared with the synthesized sample ZnO:CeO_2 (70 °C). Moreover, the diffraction lines present a narrowing of the peaks. This observation indicates that the heat treatment increases the average size of the crystallites. The average sizes of the crystallites of the prepared samples were calculated by the Scherrer formula [13], and the values are shown in Table 1. All the diffraction peaks have been considered in the calculation.

The SEM images in Fig. 2 reveal the general morphological aspect of the powder particles. The synthesis of the sol–gel system led to the formation of particles clusters of spheroidal shape. The average particle size was estimated between 50 and 100 nm for both synthesized samples. Therefore, according to crystallite size,

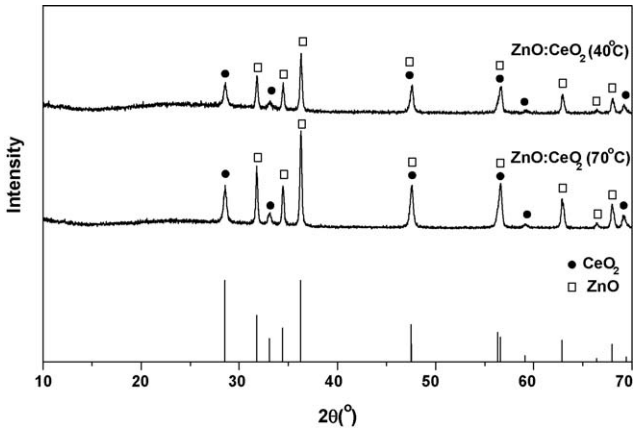

Fig. 1. X-ray diffraction patterns of CeO_2, ZnO and synthesized ZnO:CeO_2 systems (40 and 70 °C).

Table 1
Average crystallite size calculated [12] for the samples calcined at 600 °C.

Samples	Crystallite size (nm)
ZnO:CeO_2 (40 °C)	35.8
ZnO:CeO_2 (70 °C)	38.2

each spheroidal-shaped particle from the ZnO:CeO_2 system must be formed by nanocrystallites in the range from 35 to 38 nm, Table 1.

The temperature at witch the material was obtained did not influence the particle morphology, since the images for the two samples are similar.

In the powder reflection spectra, low reflectance values indicate high absorption in the corresponding wavelength region. Fig. 3 shows the reflection spectra of the ZnO:CeO_2 samples synthesized at both temperatures, as well as a comparison of these spectra with those of the pure commercial CeO_2, ZnO, and TiO_2 currently employed in the cosmetic industry. The synthesized samples have the same low reflectance behavior in the UV region, and high reflectance in the visible region. The synthesized samples display low reflectance in all UV-B region (280–320 nm), which means high absorption. Zinc oxide has the lowest reflectance rate and cerium oxide the highest, while the synthesized samples display intermediate reflection. Considering the UV-A region (320–400 nm), the synthesized samples display high absorption from 320 to 350 nm, and the reflectance starts to increase at 350 nm for all compounds; however, this behavior is more pronounced in the zinc oxide, which presents a steeper slope than all the other samples, so the synthesized samples are really promising. The synthesized samples display high reflectance from 450 nm, which means lower absorption in the visible. Therefore, mixed oxides display high absorption in the UV region (low reflectance) and high transparency in the visible region, making them promising materials in the search for sunscreen formulations and personal care products [14–16].

The conductometric method (Rancimat®) is efficient in estimating the catalytic activity of inorganic pigments used in cosmetics [10]. Fig. 4 presents the evolution of the catalytic activity as a function of time for the catalysts as well as a comparison with castor oil oxidation in the absence of catalyst.

The synthesized materials promote similar evolution in conductivity (catalytic activity), with a higher activity being observed for the sample prepared at 40 °C. The important factor for comparison between the oxides is the I_{ca} (index of catalytic activity) and whether the synthesized samples behave as antioxidant or oxidant when compared with pure castor oil in each case. The comparison should be made by analyzing the degree of catalyst activity as a function of time. The I_{ca} was estimated by the change in conductance (σ) after several hours of oxidation (1–8 h) [17] and castor oil conductance was used as the blank. The I_{ca} of the synthesized samples shown in Table 2 were normalized by the following equation:

$$I_{ca} = \frac{\sigma_{sample} - \sigma_{blank}}{\sigma_{blank}} \quad (1)$$

Table 2 shows that the ZnO:CeO_2 sample (40 °C) functioned as oxidant during all the period, while the ZnO:CeO_2 sample (70 °C) had a virtually neutral behavior, remaining as an antioxidant for short periods at times 1, 4, 5, and 6 h.

The photocatalytic activity of the prepared samples was evaluated by the change in the conductivity of water containing volatile products from to degradation of castor oil, which was heated and irradiated with light. A comparative analysis of the

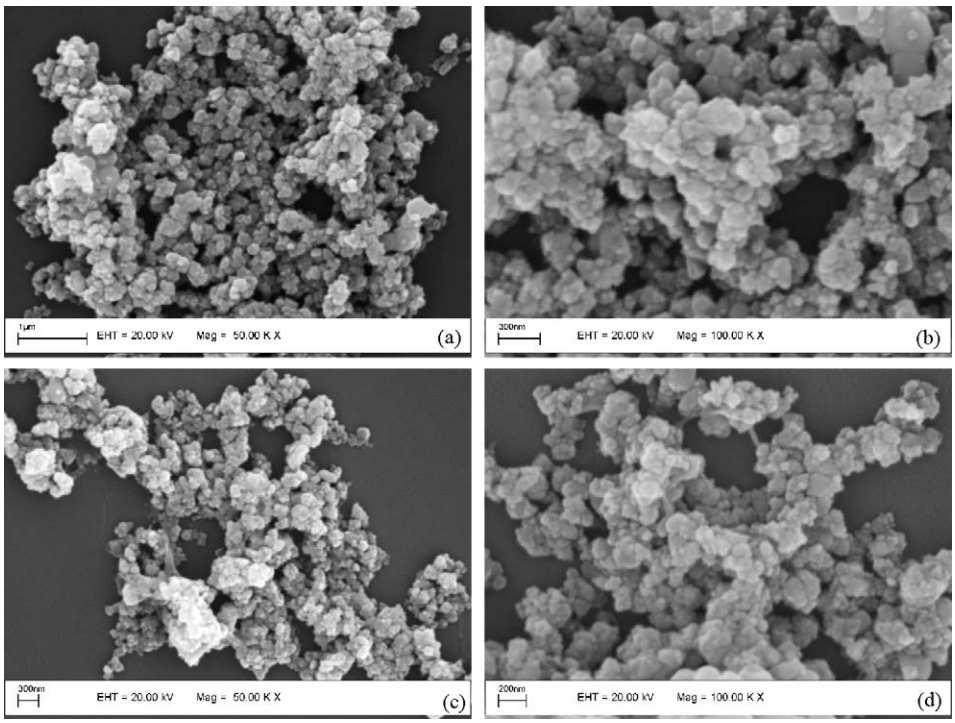

Fig. 2. SEM images of (a) and (b) ZnO:CeO_2 (70 °C) and (c) and (d) ZnO:CeO_2 (40 °C).

Table 2
Comparison of the I_{ca} of the samples.

Samples	I_{ca}							
	1 h	2 h	3 h	4 h	5 h	6 h	7 h	8 h
ZnO:CeO_2 (40 °C)	0.046	0.048	0.043	0.043	0.042	0.052	0.054	0.060
ZnO:CeO_2 (70 °C)	−0.006	0.005	0.002	−0.002	−0.010	−0.006	0	0.027

photocatalytic activity of the synthesized samples in pure castor oil is represented in Fig. 5.

The photocatalytic activities of the synthesized samples have a similar behavior during the analyzed time interval. The ZnO:CeO_2 sample (70 °C) starts to degrade the oil in about 5 h of analysis, while the ZnO:CeO_2 sample (40 °C) starts at approximately 5.5 h. The increase in conductivity was minimal during the first hours and then increased for all the samples.

The catalytic activity of ceria can be related with the oxygen evolution and absorption equilibrium reaction shown in Eq. (2):

$$CeO_2 \rightarrow Ce^{4+}{}_{1-X}Ce^{3+}{}_{X}O_{(2-X)/2}V_{oX/2} + X/4O_2 \quad (2)$$

It is well known that the ideal $r(M^{n+})/r(O^{2-})$ ionic size ratio in MO^8 eight-coordination oxide is 0.732. In the case of the ceria fluorite structure, $r(Ce^{4+})/r(O^{2+})$ is 0.703, which is smaller than the

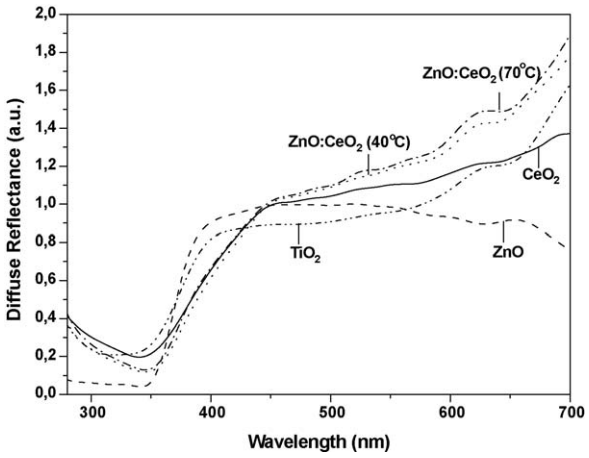

Fig. 3. Reflectance spectra of CeO_2, ZnO, TiO_2 and ZnO:CeO_2 powder systems.

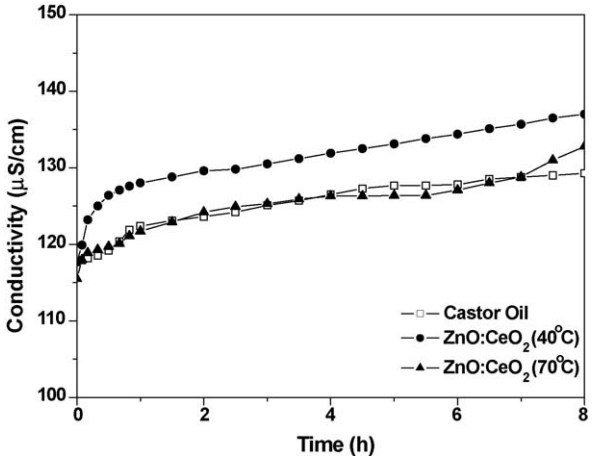

Fig. 4. Time dependence of the electric conductivity by the Rancimat® test without UV light irradiation, for castor oil with ZnO:CeO_2 (40 and 70 °C) and for pure castor oil (blank).

Table 3
I_{fca} of pure ZnO, CeO_2, TiO_2 and ZnO:CeO_2 systems.

Samples	I_{fca}							
	1 h	2 h	3 h	4 h	5 h	6 h	7 h	8 h
ZnO:CeO_2 (40 °C)	−0.056	−0.056	−0.056	−0.052	−0.023	0.020	0.073	0.152
ZnO:CeO_2 (70 °C)	−0.019	−0.022	−0.024	−0.020	0.013	0.147	0.247	0.257
ZnO	0.380	0.610	0.880	1.210	1.610	2.260	3.000	4.010
CeO_2	0.052	−0.013	0.028	0.003	−0.038	0.083	0.451	0.633
TiO_2	−0.202	−0.174	−0.034	0.201	0.841	1.263	1.852	2.552

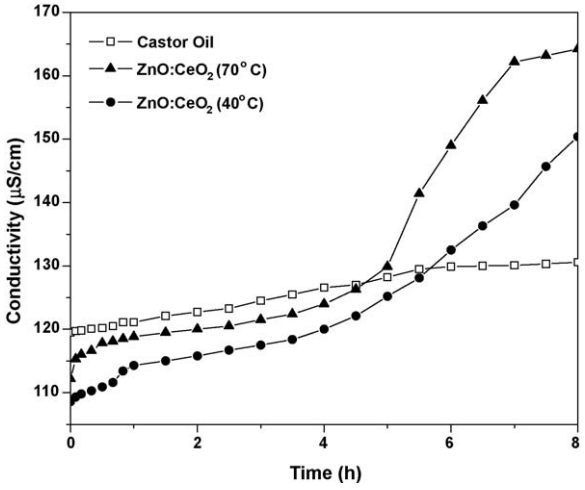

Fig. 5. Time dependence of the electric conductivity by the Rancimat® test with UV light irradiation, for castor oil with ZnO:CeO_2 (40 and 70 °C) and for pure castor oil (blank).

ideal value, indicating that Ce^{4+} is not large enough to stabilize the fluorite structure. To take on a more stable eight-coordination fluorite structure, some Ce^{4+} ions would tend to be reduced to Ce^{3+}, which has a larger ionic radius than Ce^{4+}, as shown in Eq. (2). In parallel with this reaction, oxygen molecules are released to form oxygen vacancies. Therefore, it is expected that oxygen evolution may be depressed by doping ceria with a metal ion possessing both larger ionic size and lower valence than Ce^{4+}, so as to stabilize the fluorite structure and shift the equilibrium shown in Eq. (2) to its left-hand side [7].

Table 3 shows the I_{fca} (index of photocatalytic activity) of pure ZnO, CeO_2, TiO_2 and the prepared samples. The presence of another metal ion stabilizes the structure, leading to lower conductivity values.

4. Conclusions

ZnO:CeO_2 nanopowder systems were synthesized by a non-alkoxide sol–gel procedure. The method is simple and low cost for the preparation of ultrafine particles with required characteristics. SEM analysis showed that the particles have spheroidal shape and their sizes range from 50 to 100 nm, which is appropriate for a homogeneous suspension. Moreover, ZnO:CeO_2 systems present higher UV absorption and transparency in the visible region and intermediate reflectance indices compared with pure oxides (ZnO and CeO_2). This probably implies a decrease in their pale-white resulting color.

Increasing the temperature at which the system is prepared results in a decrease in the catalytic activity for castor oil oxidation. The photocatalytic activity of ZnO:CeO_2 systems for organic material oxidation is much smaller than that of titania, ceria, and zinc oxide. Therefore, the findings of the present work suggest that the ZnO:CeO_2 systems are promising candidates for use as optical UV-filters even in the presence of organic materials.

Acknowledgements

We thank Dr. C.M.C. do Prado Manso and Dr. R.F. Silva for helpful discussions and the Brazilian agencies CAPES, CNPq, and FAPESP for financial support.

References

[1] A. Trovarelli, C. de Leitenburg, M. Boaro, G. Dolcetti, The utilization of ceria in industrial catalysis, Catal. Today 50 (1999) 353–367.
[2] E. Bekyarova, P. Formasiero, J. Kaspar, M. Graziani, CO oxidation on Pd/CeO_2–ZrO_2 catalysts, Catal. Today 45 (1998) 179–183.
[3] H. Yahiro, Y. Baba, K. Eguchi, J.H. Arai, High temperature fuel cell with ceria–yttria solid electrolyte, Electrochem. Soc. 135 (1988) 2077–2080.
[4] N. Izu, W. Shin, N. Murayama, S. Kanzaki, Resistive oxygen gas sensors based on CeO_2 fine powder prepared using mist pyrolysis, Sens. Actuators B: Chem. 87 (2002) 95–98.
[5] S. Tsunekawa, R. Sahara, Y. Kawazoe, A. Kasuya, Origin of the blue shift in ultraviolet absorption spectra of nanocrystalline CeO_2 particles, Mater. Trans. JIM 41 (2000) 1104–1107.
[6] S. Yabe, M. Yamashita, S. Momose, K. Tahira, S. Yoshida, R. Li, S. Yin, T. Sato, Synthesis and UV-shielding properties of metal oxide doped ceria via soft chemical route, Int. J. Inorg. Mater. 3 (2001) 1003–1008.
[7] R. Li, S. Yabe, M. Yamashita, S. Momose, S. Yoshida, S. Yin, T. Sato, UV shielding properties of zinc oxide-doped ceria fine powders derived via soft solution chemical routes, Mat. Chem. Phys. 75 (2002) 39–44.
[8] F. Cheviré, F. Muñoza, C.F. Bakera, F. Tessiera, O. Larchera, S. Boujdayb, C. Colbeau-Justinb, R. Marchanda, UV absorption properties of ceria-modified compositions within the fluorite-type solid solution CeO_2–Y_6WO_{12}, J. Solid State Chem. 179 (2006) 3184–3190.
[9] M.G. Sujana, K.K. Chattopadyay, S. Anand, Characterization and optical properties of nano-ceria synthesized by surfactant-mediated precipitation technique in mixed solvent system, Appl. Surf. Sci. 254 (2008) 7405–7409.
[10] J.-S. Lee, S.-C. Choi, Crystallization behavior of nano-ceria powders by hydrothermal synthesis using a mixture of H_2O_2 and NH_4OH, Mater. Lett. 58 (2004) 390–393.
[11] D. Moya, J.L. Refrégier, A. Chardon, In vivo measurement of the photostability of sunscreen products using diffuse reflectance spectroscopy, Photodermatol. Photoimmunol. Photomed. 18 (2002) 14–22.
[12] Powder Diffraction File PDF-2 database sets 1–44. Pennsylvania: Joint Committee on Powder diffraction Standards—International Center for Diffraction Data, c 1988, PDF numbers 75-0390 (CeO_2), 80-0074 (ZnO), CD-ROM.
[13] B. Cullity, Elements of X-ray Diffraction, 2ª Edição, Addison-Wesley, Redding, MA, 1978.
[14] M.A. Mitchnick, D. Fairhurst, S.R. Pinnel, Microfine zinc oxide (Z-cote) as a photostable UVA/UVB sunblock agent, J. Am. Acad. Derm. 40 (1999) 85–90.
[15] H. Wang, J.J. Zhu, X.H. Liao, S. Xu, T. Ding, H.Y. Chen, Preparation of nanocrystalline ceria particles by sonochemical and microwave assisted heating methods, Phys. Chem. Chem. Phys. 4 (2002) 3794–3799.
[16] G.P. Dransfield, Inorganic sunscreens, in: Proceedings of the International Workshop on UV Exposure, Measurement and Protection, vol. 91, Oxford. Radiat. Prot. Dosim, 18–20 October 1999, (2000), pp. 271–273.
[17] T. Masui, M. Tamamoto, T. Sakata, M. Hirotaro, A. Gin-ya, Synthesis of BN coated CeO_2 fine powder as a new UV blocking material, J. Mater. Chem. 10 (2000) 353–357.